A Combinatorial Biophysical approach; FTSA and SPR for identifying Small Molecule Ligands and PAINs.

ARTICLE *in* ANALYTICAL BIOCHEMISTRY · MARCH 2015

Impact Factor: 2.22 · DOI: 10.1016/j.ab.2015.03.013 · Source: PubMed

8 AUTHORS, INCLUDING:

Rupert Satchell

Sygnature Discovery

1 PUBLICATION **0** CITATIONS

SEE PROFILE

Vytautas Petrauskas

Vilnius University

32 PUBLICATIONS **62** CITATIONS

SEE PROFILE

Daumantas Matulis

Vilnius University

80 PUBLICATIONS **1,668** CITATIONS

SEE PROFILE

John Unitt

Sygnature Discovery

31 PUBLICATIONS **1,478** CITATIONS

SEE PROFILE

Analytical Biochemistry 479 (2015) 63–73

Contents lists available at ScienceDirect

Analytical Biochemistry

journal homepage: www.elsevier.com/locate/yabio

A combinatorial biophysical approach; FTSA and SPR for identifying small molecule ligands and PAINs

M. Redhead [a,*], R. Satchell [a], V. Morkūnaitė [c,d], D. Swift [a], V. Petrauskas [c], E. Golding [a], S. Onions [b], D. Matulis [c,*], J. Unitt [a,*]

[a] Bioscience Department, Sygnature Discovery, BioCity, Nottingham NG1 1GF, UK
[b] Chemistry Department, Sygnature Discovery, BioCity, Nottingham NG1 1GF, UK
[c] Department of Biothermodynamics and Drug Design, Institute of Biotechnology, Vilnius University, Vilnius LT-02241, Lithuania
[d] Department of Neurobiology and Biophysics, Faculty of Natural Sciences, Vilnius University, Vilnius 03101, Lithuania

ARTICLE INFO

Article history:
Received 31 October 2014
Received in revised form 6 March 2015
Accepted 11 March 2015
Available online 30 March 2015

Keywords:
FTSA
SPR
Biophysics
Drug discovery
Assay interference
Screening

ABSTRACT

Biophysical methods have emerged as attractive screening techniques in drug discovery both as primary hit finding methodologies, as in the case of weakly active compounds such as fragments, and as orthogonal methods for hit validation for compounds discovered through conventional biochemical or cellular assays. Here we describe a dual method employing fluorescent thermal shift assay (FTSA), also known as differential scanning fluorimetry (DSF) and surface plasmon resonance (SPR), to interrogate ligands of the kinase p38α as well as several known pan-assay interference compounds (PAINs) such as aggregators, redox cyclers, and fluorescence quenchers. This combinatorial approach allows for independent verification of several biophysical parameters such as K_D, k_{on}, k_{off}, ΔG, ΔS, and ΔH, which may further guide chemical development of a ligand series. Affinity values obtained from FTSA curves allow for insight into compound binding compared with reporting shifts in melting temperature. Ligand–p38 interaction data were in good agreement with previous literature. Aggregators and fluorescence quenchers appeared to reduce fluorescence signal in the FTSAs, causing artificially high shifts in T_m values, whereas redox compounds caused either shifts in affinity that did not agree between FTSA and SPR or a depression of FTSA signal.

Biophysical methods of interrogating the binding of putative ligands offer various advantages over their biochemical and cellular counterparts [1]. Techniques such as surface plasmon resonance (SPR)[1] [2], isothermal titration calorimetry (ITC) [3], and fluorescent thermal shift assay (FTSA) [4] measure the direct effect of ligands binding to a protein; therefore, specific reagents such as fluorescent displacement probes and artificial substrates (e.g., peptides with cleavable fluorophores for enzymatic assays) do not need to be generated. The above techniques infer compound binding only as a direct effect of the readout as opposed to a secondary effect such as enzyme inhibition or second messenger production, allowing for greater confidence in determining the affinity of weak binders. Weak binders are often screened at concentrations that may interfere with traditional fluorescence assays by mechanisms such as compound autofluorescence and quenching [5,6] as well as aggregation that may inhibit enzymatic activity [7] and cause nonspecific G-protein-coupled receptor inhibition [8]. Biophysical techniques also show utility within the validation of hits obtained using traditional biochemical or cellular screens. High-throughput screening using classical biochemical or cellular methodologies is known to identify a number of undesirable pan-assay interference compounds (PAINs) that do not match the effect of real ligands in biophysical screens [7,9]. Compounds that progress through hit-to-lead and lead optimization may also benefit from biophysical technique as further interrogation of binding than simple affinity may allow for fine-tuning of molecular interaction. Modification of molecular interactions can be included in terms of extended residence time to improve pharmacokinetics/pharmacodynamics [10]. Thermodynamic categories of interaction may also be considered; enthalpically driven hydrogen bonding or π–π stacking, rather than less specific entropically driven interactions

* Corresponding authors.
E-mail addresses: m.redhead@sygnaturediscovery.com (M. Redhead), daumantas.matulis@bti.vu.lt (D. Matulis), j.unitt@sygnaturediscovery.com (J. Unitt).

[1] *Abbreviations used:* SPR, surface plasmon resonance; ITC, isothermal titration calorimetry; FTSA, fluorescent thermal shift assay; PAIN, pan-assay interference compound; DSC, dynamic scanning calorimetry; qPCR, quantitative real-time polymerase chain reaction; DLS, dynamic light scattering; DTT, dithiothreitol; DMSO, dimethyl sulfoxide; PBS, phosphate-buffered saline; CAC, critical aggregation concentration; NTA, nitrilotriacetic acid; HBS, Hepes and NaCl (pH 7.4); NHS, *N*-hydroxysuccinimide; EDC, 1-ethyl-3-(3-dimethylaminopropyl)carbodiimide hydrochloride.

http://dx.doi.org/10.1016/j.ab.2015.03.013
0003-2697/

[11–13], may present as a useful tool for querying and improving medicinal chemistry design and experiments.

Biophysical techniques are, however, not without limitations; ITC and FTSA have relatively high protein requirements when compared with traditional biochemical experiments [14], often microgram to milligram quantities per data point. FTSA can require up to 25-fold less protein than ITC [4], yet FTSA still can require micromolar concentrations of protein. Furthermore, although SPR has much lower protein requirements than ITC and FTSA [15], all three techniques have a much lower throughput than traditional biochemical assays [1]. During measurement with the above techniques, single data points can take several minutes and are often run in tandem rather than in parallel. FTSA offers a higher throughput analogous technology to dynamic scanning calorimetry (DSC) [4]. DSC detects phase transitions, such as the melting of a protein, by measuring the difference in energy required to heat a sample compared with a control [16]. Rather than a direct measurement of energy input, FTSA employs an environmentally sensitive dye, the fluorescence of which increases in hydrophobic environments such as the core of proteins that are exposed during melting. FTSA, therefore, requires lower protein concentrations (often only hundreds of nanograms per data point) (Table 1).

True ligands stabilize protein structure and impede thermal denaturation [4,16–19]. Hence, a binding interaction can be inferred when the temperature at which a protein melts across a thermal gradient increases in the presence of a ligand. FTSA experiments may be performed in a thermal cycler suitable for reverse transcription–quantitative real-time polymerase chain reaction (RT–qPCR); therefore, large numbers of samples may be run in parallel [4,17,19].

To demonstrate the utility of these techniques to the drug discovery scientist, the model protein p38α was selected. p38α has been well characterized previously in the literature and has several well-known small molecule ligands that exhibit different, well-understood molecular binding mechanisms [20–23]. These ligands include simple ATP competitive ligands in the SB prefix series (Fig. 1, compounds **5**–**7**) [20,21,23] or the tight binding allosteric BIRB 796 compound (Fig. 1, compound **1**) [22]. Three fragments of BIRB 796 were also assessed (Fig. 1, compounds **2**–**4**), the binding of which was predicted by structure similarity. These selections allowed verification of results against other methods within the literature as well as invite critique within a familiar system.

To determine the profiles of PAINs within FTSA, several compounds known to cause interference in biochemical and cellular assays were selected (Fig. 1, compounds **8**–**13**). Four common mechanisms of assay interference were chosen for study: promiscuous aggregation [24], redox cycling [9], fluorescence quenching [25], and chelation [26]. Rottlerin and Congo Red were chosen as promiscuous aggregators (Fig. 1, compounds **8** and **9**) [27,28]. These compounds form nanoparticles in solution that are able to sequester protein onto their surface, causing nonspecific inhibition of enzyme activity and protein–protein interactions [27]. To confirm formation of nanoparticles, dynamic light scattering (DLS) was employed [29]. Redox cycling compounds PR-619 and benzoquinone (Fig. 1, compounds **11** and **12**) were selected [30,31]. Redox cyclers can cause oxidation of cysteine residues on the

Table 1
Typical protein requirements for biophysical and biochemical assays within Sygnature Discovery.

Assay	Protein concentration	Volume
SPR	fM (on chip) 100–1000 nM (coupling)	100 µl (coupling)
FTSA	100–6000 nM	3–20 µl
ITC	25–75 µM	Up to 2.1 ml
FRET/AlphaScreen	10–100 nM	5–30 µl
Enzymatic	0.05–1000 nM	10–100 µl
Receptor binding	10–1000 nM	10–100 µl

Note. FRET, fluorescence resonance energy transfer.

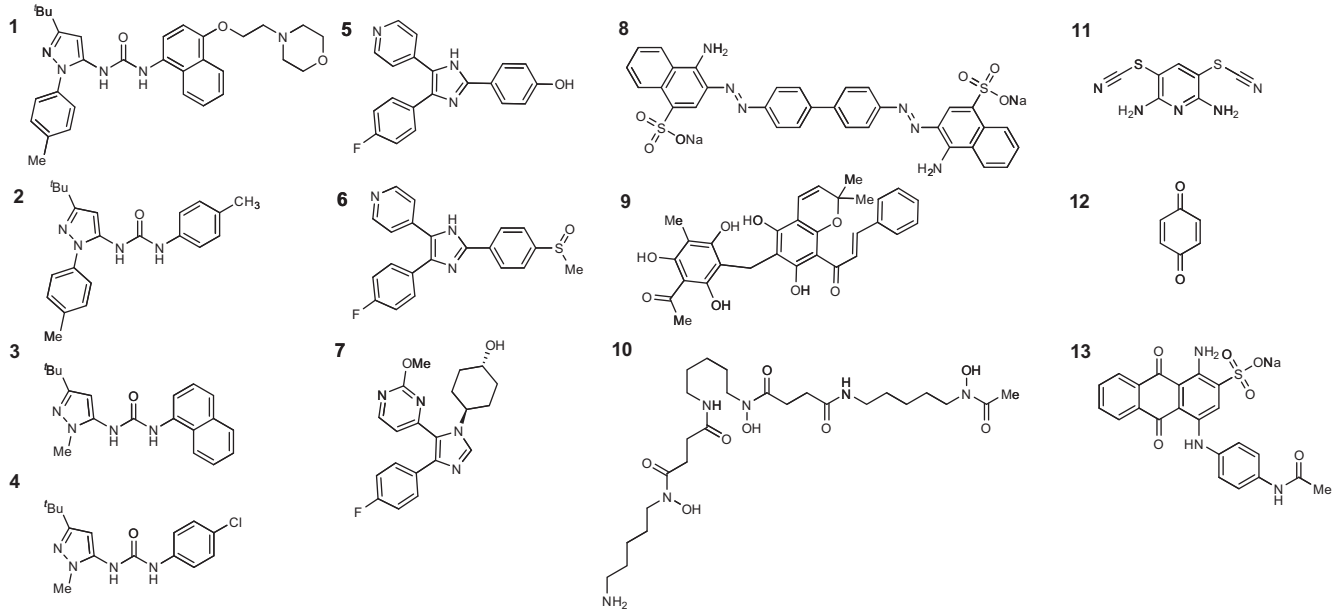

Fig.1. Structures of the compounds tested. Compounds **1** to **4** represent **1** (p38 inhibitor BIRB796) and **2**–**4** (fragments of its structure). Compounds **5** to **7** are the pyridinyl imidazole p38 inhibitors SB202190, SB203580, and SB239063. Compounds **8** to **13** are interference compounds (**8** and **9** are the aggregators Congo Red and rottlerin, **10** is the chelator deferoxamine, **11** and **12** are redox cyclers PR-619 and benzoquinone, and **13** is the fluorescence quencher acid blue 40).

structure of proteins, causing inhibition of enzyme activity as well as producing hydrogen peroxide when in aqueous solution, which may interfere with oxygen radical-based assay technologies such as AlphaScreen [9]. PR-619 is a Michael acceptor and, thus, is able to nonspecifically label cysteine residues [31]. Confirmation of compound redox cycling was measured by compound ability to catalyze the reduction of resazurin by dithiothreitol (DTT) [9]. Acid blue was selected as a fluorescence quencher, and deferoxamine as a metal ion chelator (Fig. 1, compounds **10** and **13**) [32].

Materials and methods

Materials

Compounds **1**, **5**, **6**, and **7** were obtained from Tocris (Bristol, UK), compound **2** was obtained from Enamine (Monmouth Junction, NJ, USA), compounds **3** and **4** were obtained from Thermo Fisher (Loughborough, UK), and compounds **8** to **13** were obtained from Sigma Aldrich (Poole, UK). All compounds were acquired as solid samples (>95% purity) and dissolved in dimethyl sulfoxide (DMSO) as required. All SPR sensor chips were obtained from General Electric Life Sciences (Abingdon, UK). SYPRO Orange dye was obtained from Life Technologies (Paisley, UK). Human recombinant, full-length, His-tagged inactive p38α was obtained from R&D Systems (Abingdon, UK). All other reagents were purchased from Sigma–Aldrich (Poole, UK).

Methods

DLS

Compounds were serially diluted 10-fold from 10 mM DMSO stocks into DMSO to give eight concentrations from 10 to 0.1 mM. This dilution series was diluted in phosphate-buffered saline (PBS) that had been 2 μm filtered and degassed by sonication to give a concentration range from 100 to 1 μM in PBS with 1% (v/v) DMSO.

DMSO (1%, v/v) in PBS was used as negative control for particle formation. These solutions were then measured using a Zetasizer Nano plate-based DLS reader (Malvern, Malvern, UK). Correlograms were compared and used to determine radii of any particles present. The critical aggregation concentration (CAC) for solutions that formed particles was determined by fitting the intensity of scattered light to concentration (static light scattering) using the conditional Eq. (1):

$$Y_r = IF(L_T < \mathrm{CAC}, Y_{r0}, Y_{r0} + k_{\mathrm{agg}} \cdot (L_T - \mathrm{CAC})), \tag{1}$$

where Y_r is the response measured, Y_{r0} is the baseline response, k_{agg} is the rate at which light is scattered when compared with concentration, and L_T is the total ligand concentration.

Resazurin assay

Resazurin assay for redox cycling compounds was performed as described previously [9].

FTSA

Protein FTSAs were performed using the Protein Thermal Shift Dye Kit (Life Technologies) in MicroAmp Optical Reaction Plates. Compounds were diluted from 10 mM DMSO stocks in DMSO. The DMSO solution containing compound was diluted 25-fold in assay buffer (50 mM Hepes, 125 mM NaCl, and 100 μM ethylenediaminetetraacetic acid [EDTA], pH 7.6) before being diluted 4-fold into assay buffer to give a concentration range of 30 nM to 100 μM with 1% (v/v) DMSO. Each assay contained 0.47 μM p38α and SYPRO Orange at a final dilution of 1000-fold from the supplier's stocks to a final volume of 20 μl in assay buffer. His-tagged p38α, SYPRO Orange, and 1% (v/v) DMSO in assay buffer were used to determine the thermal profile of the native protein. SYPRO Orange and 1% (v/v) DMSO in assay buffer were used to determine fluorescent profiles observed solely due to the melt behavior of His-tagged p38α. Following compound addition, plates were equilibrated at room temperature for 60 min. Reactions were performed in a StepOnePlus Real-Time PCR System (Life Technologies), with heating at a rate of 2 °C min^{-1} across a gradient between 25 and 95 °C.

Analysis of melting curves. Fluorescence traces from FTSA were analyzed as described previously in Refs. [4,17,18]. Briefly, fluorescence (y) dependence on temperature (T) follows this equation:

$$y(T) = y_{F,T_m} + m_F(T - T_m) + \frac{(y_{U,T_m} - y_{F,T_m}) + (m_U - m_F)(T - T_m)}{1 + e^{(\Delta_U H_{T_m} + \Delta_U C_p (T - T_m) - T(\Delta_U S_{T_m} + \Delta_U C_p \ln(T/T_m)))/RT}}, \tag{2}$$

where y_{F,T_m} is the fluorescence of the probe bound to folded native protein before transition at T_m, y_{U,T_m} is the fluorescence of the probe bound to the unfolded protein after unfolding transition at T_m, m_F is the slope of the fluorescence dependence on temperature when the probe is bound to the native protein, and m_U is the slope of fluorescence dependence on temperature when the probe is bound to the unfolded protein. The linear dependence of the probe fluorescence on temperature is only the first approximation. In reality, the dependence of the probe fluorescence on temperature has nonlinear dependence. $\Delta_u H_{Tm}$ is the enthalpy of unfolding, $\Delta S_u H_{Tm}$ is the entropy of unfolding, and $\Delta_u C_p$ is the change in heat capacity on unfolding, assumed to be temperature independent in the studied temperature range. Fluorescence traces from FTSA are roughly sigmoidal (described by Eq. (2)) with sloped upper and lower asymptotes that may be mathematically described as a simple linear relationship between fluorescence and temperature. Tight binding ligands may appear as a biphasic sigmoid that is best described by the following equation:

$$y = a_f + b_f \cdot (x - T_r) \cdot + c_f \cdot (x - T_r)^2 + (a_u - a_f + (b_u - b_f) \cdot (x - T_r) + (c_u - c_f) \cdot (x - T_r)) \cdot \left(\frac{1 - n}{1 + exp^{\frac{(\Delta H_{\mathrm{free}} + \Delta_u C_p \cdot (X - T_{m\mathrm{free}})) - x\left(\Delta S_{\mathrm{free}} + \Delta_u C_p \cdot \ln\left(\frac{X}{T_{m\mathrm{free}}}\right)\right)}{R \cdot T}}} \right) + \left(\frac{1 - n}{1 + exp^{\frac{(\Delta H_{\mathrm{bound}} + \Delta_u C_p \cdot (X - T_{m\mathrm{bound}})) - x\left(\Delta S_{\mathrm{bound}} + \Delta_u C_p \cdot \ln\left(\frac{X}{T_{m\mathrm{bound}}}\right)\right)}{R \cdot T}}} \right), \tag{3}$$

where a_f, b_f, and c_f describe the slope of the lower asymptote, a_u, b_u, and c_u describe the slope of the upper asymptote, T_r is an arbitrary reference temperature (e.g., 298.15 K), ΔH_{free}, ΔS_{free}, and $T_{m\mathrm{free}}$ describe the enthalpy, entropy, and melting transition temperature of the free protein, and $\Delta H_{\mathrm{bound}}$, $\Delta S_{\mathrm{bound}}$, and $T_{m\mathrm{bound}}$ describe the enthalpy, entropy, and melting transition temperature of the ligand-bound protein.

Ligands of a protein stabilize the structure on binding, leading to enhanced thermal stability, hence the protein transitions to the unfolded state at a higher temperature. This effect may be thought of as a pair of competing equilibria given by Eq. (4):

$$[U] + [L] \overset{K_u}{\rightleftharpoons} [N] + [L] \overset{K_b}{\rightleftharpoons} [NL], \tag{4}$$

where native protein, [N], may either unfold to unfolded protein, [U], or bind to its ligand, [L], forming a complex of liganded protein [NL]. The equilibrium constants for unfolding and binding are given by K_u and K_b, respectively.

The concentration of a ligand (L_t) to be added in order to raise the protein melting temperature from T_r (reference temperature, e.g., 60 °C) to T_m may be estimated using the following equation:

$$L_t = \left(e^{-\left(\Delta_U H_{T_r}+\Delta_U C_p(T_m-T_r)-T_m\left(\Delta_U S_{T_r}+\Delta_U C_p \ln(T_m/T_r)\right)\right)/RT_m} - 1\right) \times \left[\frac{P_t}{2}\frac{1}{e^{-\left(\Delta_U H_{T_r}+\Delta_U C_p(T_m-T_r)-T_m\left(\Delta_U S_{T_r}+\Delta_U C_p \ln(T_m/T_r)\right)\right)/RT_m}} + \frac{1}{e^{-\left(\Delta_b H_{T_0}+\Delta_b C_p(T_m-T_0)-T_m\left(\Delta_b S_{T_0}+\Delta_b C_p \ln(T_m/T_0)\right)\right)/RT_m}}\right], \quad (5)$$

where P_t is the total protein concentration and T_0 is the reference temperature (e.g., 37 °C) for which the ligand binding constant is to be determined.

SPR

Immobilization of inactive p38α. SPR experiments were performed using a Biacore T200 system (GE Healthcare) equipped with a research-grade NTA (nitrilotriacetic acid) sensor chip. p38α was immobilized using capture/coupling amine chemistry.

The instrument was primed with 10 mM Hepes and 150 mM NaCl (pH 7.4) (HBS) to allow surface equilibration and protein immobilization carried out at a flow rate of 10 μl min^{-1}. EDTA (350 mM) was injected over the surface for 60 s, followed by an injection of HBS for 120 s. The chip was preconditioned with an injection of 0.5 M $NiCl_2$ for 60 s, and the surface was activated with *N*-hydroxysuccinimide (NHS) and 1-ethyl-3-(3-dimethylaminopropyl)carbodiimide hydrochloride (EDC) (Amine Coupling Kit, GE Life Sciences). NHS/EDC (5.8 mg ml^{-1} NHS + 37.5 mg ml^{-1} EDC) was injected for 420 s at a flow rate of 10 μl min^{-1} to derivatize the carboxymethylated dextran surface with reactive NHS ester groups. Inactive p38α was diluted in HBS containing 10 μM compound **6** to protect primary amines at the compound binding site from reacting with the derivatized surface. Remaining NHS esters were blocked with a 420 s injection of ethanolamine. The active flow cell surface was immobilized at a density of approximately 4500 RU per immobilization.

To collect kinetic binding data, the analyte (compounds **5**–**7**) in running buffer (50 mM Tris, 150 mM NaCl, 10 mM $MgCl_2$, 1 mM $MnCl_2$, and 5% [v/v] DMSO, pH 7.5) was injected over the two flow cells at concentrations between 2 and 1000 nM at a flow rate of 30 μl min^{-1} over set temperatures along a gradient between 4 and 37 °C for compounds **5** to **7** and at 37 °C only for compounds **1** to **4**. The PAIN compounds **8** to **13** were prepared as above at concentrations between 1 and 100 μM and assayed at 25 °C.

Each sample was injected over the flow cell once, with sample concentrations (62.5 nM) injected twice, and a buffer blank was flowed over the two surfaces on two separate occasions. Data were collected at a rate of 10 Hz. The data were fitted to a simple 1:1 interaction model using the global data analysis option available within Biacore T200 evaluation software (GE Life Sciences).

The PAIN compounds **8** to **13** were prepared as above at concentrations between 1 and 100 μM and assayed at 25 °C.

Single cycle kinetics. Compounds **1** to **7** in running buffer were injected over the two flow cells at concentrations between 7 and 900 nM in subsequent injections across a single cycle at a flow rate of 30 μl min^{-1} over a temperature gradient from 4 to 37 °C. The complex was allowed to associate for 60 s for each of the five injections, followed by a measured dissociation phase of up to 1800 s. Data were collected at a rate of 10 Hz. The data were fit to a simple 1:1 interaction model using the Biacore T200 evaluation software.

Results

DLS results

DLS uses the change in intensity of scattered light over time to calculate the size of nanometer-scale particles in solution. Small molecules that aggregate to form 10- to 1000-nm particles in solution may interfere with biochemical and biophysical assays by sequestering protein onto their surfaces, resulting in nonspecific inhibition or false positives for binding. Of the compounds tested, there was evidence of particle formation at the highest concentration (100 μM) tested for nearly all compounds (Fig. 2). This was unsurprising given that DLS methods may be more sensitive to precipitation of compounds that are approaching their solubility limit than optical density or nephelometry-based assays [33]. CAC values were obtained for the compounds by comparing the intensity of scattered light to concentration using Eq. (1). Intensity of scattered light serves as a better measure for CAC than particle size because size may not correlate with concentration; instead, the number of particles may increase or heterogeneous solutions of particles and larger precipitate aggregates (>1000 nM) may confuse results.

Resazurin assay results

The resazurin assay is able to detect redox cycling by compounds via reduction of resorufin to resazurin either via direct cycling with the reducing agent DTT or by production of hydrogen peroxide in solution. Of the compounds tested, only the Michael acceptor compound **11** and the redox cycler compound **12** produced a positive response in this assay (Fig. 3).

FTSA results

On heating, p38α displayed a single melting transition. This resulted in an increased SYPRO fluorescence centered on the T_m of the protein at 43 °C (Fig. 4). Eq. (2) was fitted to the raw fluorescence data, from which the thermodynamic parameters of the p38α melting transition were established (Table 2).

Reversible ligands of p38α, compounds **1** to **7**, raised the temperature at which the melting transition occurred, and T_m values were readily obtained using either Eq. (2) (compounds **2**–**6**) (Fig. 4) or Eq. (3) (compound **1**) (Fig. 5). Compound affinity was determined by fitting the ligand concentration needed to cause experimentally derived T_m shifts using Eq. (5) (Fig. 4), the values of which are summarized in Table 3.

The PAIN compounds **8** to **13** had differential effects on the FTSA curves depending on their mechanism of interference. The promiscuous aggregators Congo Red and rottlerin caused sharp decreases in fluorescence from above their CAC (Fig. 6). It was possible to fit apparent K_D values for the compounds; however, investigators should be wary of this because Eq. (5) is based on the 1:1 binding equilibrium displayed in Eq. (4). The formation of nanoparticles by promiscuous aggregators results from of a great number of molecules that in turn may sequester several protein molecules, leading to super-stoichiometric interactions that are not accounted for in the model. Regardless, nonspecific protein aggregation is likely to be an intractable molecular mechanism for generation of a viable therapeutic; thus, compounds showing these effects should be discarded or a least treated with great caution.

A similar profile was seen for compound **13** (Fig. 6), the fluorescence quencher acid blue. In this case, increasing compound concentration served to quench signal from the assay. Again, K_D values could be derived from fitted curve but do not correspond

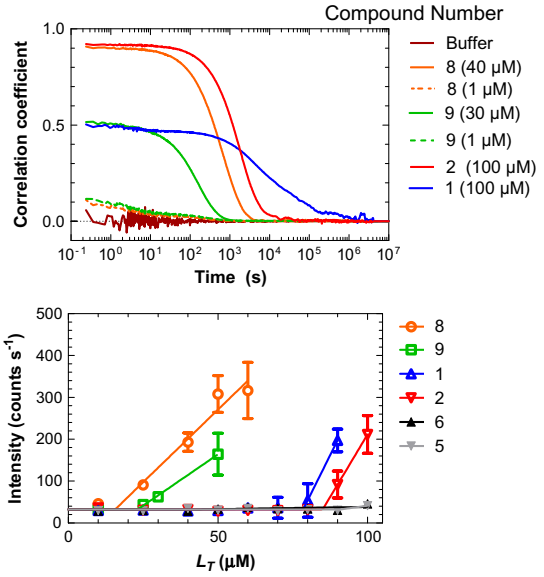

Fig.2. Example DLS data. The upper graph shows correlograms obtained for a number of compounds above and below their CACs and a measurement for the signal from buffer alone. Data are single measurements representative of three repeats. The lower graph shows the change in intensity of scattered light against ligand concentration fitted to Eq. (1) to calculate CAC values. Data are shown as means ± standard deviations ($n \geqslant 2$).

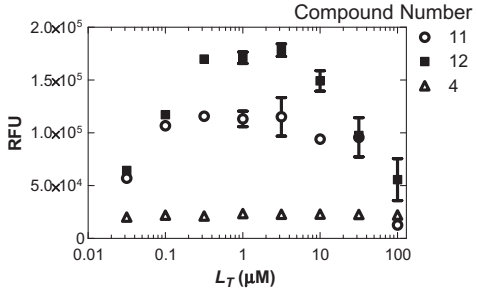

Fig.3. Differential effects of compounds on catalysis of DTT-mediated reduction of resazurin to fluorescent resorufin. Compounds **11** and **12** catalyzed the reaction due to their redox cycling property, whereas compound **4** had no effect. Data are means ± standard deviations ($n = 4$).

to a real binding event. Of the different PAIN mechanisms tested, fluorescence quenching is typically the easiest to identify due to the intense coloration of the compounds.

The two redox compounds **11** and **12** showed different profiles in FTSA, likely due to their different redox behaviours (Fig. 6). Compound **12**, which generates H_2O_2 in solution via a redox cycling reaction with reducing agents such as DTT, can cause oxidation of protein cysteine residues. However, this did not have an effect on protein melting. This is likely due to the relatively small changes to protein tertiary structure on oxidation of the cysteine sulfhydryl to sulfinic and sulfonic oxidation states. It was noted that fluorescence was reduced, likely due to oxidative modification of SYPRO Orange, preventing fluorescence. Compound **11** showed an increase in T_m in response to compound concentration. This is not surprising because compound **11** is a Michael acceptor that may nonspecifically label cysteine residues. Although this irreversible oxidation may be undesirable, in certain situations due to lack of target selectivity this may be used as a starting point for ligand design. The selective reversible USP7 inhibitor P22077 was developed from the nonselective compound **11**. The chelator compound **10**, deferoxamine, did not show an effect in this assay because p38α does not have a specific metal ion binding requirement; however, chelators may have a more significant effect for targets that require metal ions such as metalloenzymes.

SPR results

SPR sensorgrams were compared for a blank NTA surface and an NTA surface to which His-tagged p38α had been covalently tethered using a capture–couple method. Ligands of the p38 protein caused a greater increase in response on the p38α tethered surface as compared with the blank surface, indicating a binding event. Affinity was obtained by fitting the data to a 1:1 binding model from which k_a, k_d, and ultimately K_D values were obtained (Fig. 7). Equivalent data for the kinetic parameters were obtained regardless of whether multi- or single-cycle kinetics was employed (Fig. 7). Over a temperature gradient, k_a and k_d increased asymmetrically, which ultimately led to an increase in K_D. These data were transformed and fitted to either Eyring or Van't Hoff plots to generate thermodynamic parameters for compound p38α binding or thermodynamic activation parameters for the association and dissociation phases (Fig. 8).

The promiscuous aggregator compounds **8** and **9** showed non-stoichiometric binding, as previously described [7]. The redox cycler compound **12** did not show a response, whereas the Michael acceptor compound **11** showed concentration-independent association and no discernible dissociation, likely due to the available cysteine residues becoming saturated following labeling with the compound. The chelator compound **10** showed large responses relative to its calculated R_{max} on both the reference and analyte flow cells, likely due to binding to the NTA chip, and the fluorescence quencher compound **13** did not show an effect.

Discussion

The interactions between p38α and its various inhibitors is one of the most intensely studied systems for kinase inhibition in drug discovery [34–36], with large numbers of ligands already developed into drugs [20–23]. The vast quantities of existing data for validated ligands over a range of potencies make p38α an excellent model system for the development and validation of new methodology. The binding profiles of molecules of the SB series (compounds **5**–**7**) have been determined by a variety of biochemical and biophysical methods [20,21,23]. The efficacy of these ligands has also been established in cellular and animal systems, including inflammation [23] and cancer proliferation [37]. Although in one instance compound **6** has previously been reported in SPR and FTSA, FTSA was used only to report an increase in thermal stability rather than generation of affinity data [38]. BIRB796 (**1**) has also been studied extensively, with Structure Activity Relationship (SAR) for the series described previously using SPR [22]. The affinity of compound **1** has previously been profiled by FTSA, although it was reported only as a temperature shift rather than affinity [39], as well as in a similar study involving DSC [40]. The fragments of BIRB796 (compounds **2**–**4**) have not, to our knowledge, been reported previously as ligands of p38 and were found by structure similarity search of commercial compound databases. Compounds **2** to **4** may represent novel starting points for the generation of a new chemical series of p38 kinase inhibitors.

Small molecule affinity for a protein target by FTSA has previously been compared with ITC [4], an orthogonal calorimetric technique; however, to our knowledge, this is the first time the behavior of a test set of compounds has been compared between FTSA and SPR.

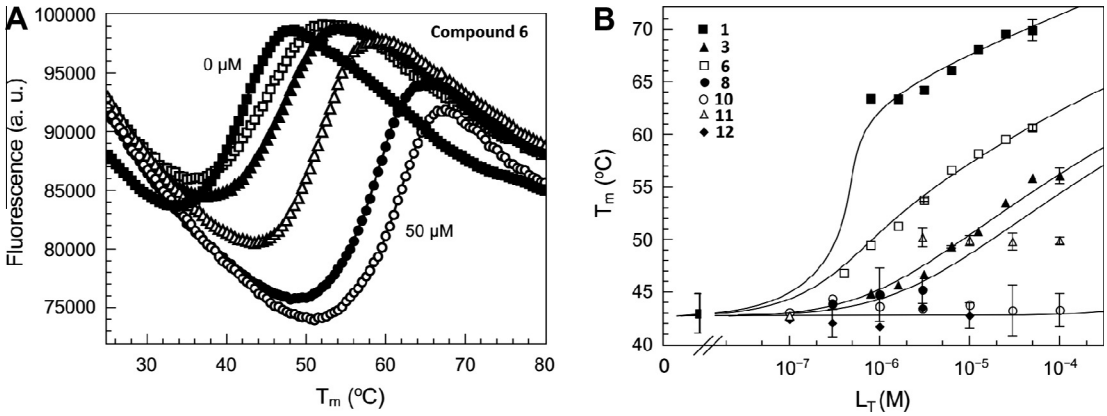

Fig.4. Example data for FTSA ligand binding assays. Panel A shows the effect of temperature on SYPRO Orange fluorescence in a system containing p38α protein and various concentrations of the ligand SB203580 (compound **6**). As the concentration of compound **6** increases, the temperature at which the melting transition occurs increases, as indicated by change in temperature where the increase in fluorescence occurs. Data are singlicate points representative of three repeats. Panel B shows the effect of total ligand concentration on melting temperature for compounds **1**, **3**, and **6**, which acted as real ligands of the p38 protein, and compounds **8**, **10**, **11**, and **12**, which were assay interference compounds. The stabilization energy is used to generate K_D values for the compounds, with compound **1** showing a large shift at 500 nM, which is equal to the protein concentration indicating tight binding. Data are means ± standard deviations ($n \geqslant 3$). Lines were fitted according to Eq. (5).

Table 2
Thermodynamic parameters of p38α thermally induced unfolding.

Parameter name	Value
$\Delta_u H$	570 ± 30 (kJ M^{-1})
$\Delta_u S$	1.8 ± 0.09 (kJ K^{-1} M^{-1})
ΔC_p	30 ± 12 (kJ M^{-1})
T_m	43 ± 0.6 °C

FTSA and SPR represent very different methods for determining compound affinity; SPR relies on pseudo-first-order (association phase) and pseudo-zeroth-order (dissociation phase) interactions to determine affinity (or by plotting the surface response at steady state to an isotherm in the absence of measurable kinetic rates). Because the femtomolar quantities of protein tethered to the chip will not likely significantly alter the free ligand concentration during association [15], equally the femtomolar quantities of bound ligand will not likely significantly raise the ligand concentration during their dissociation into buffer or undergo rebinding to the surface; therefore, the observed rates measured during the association and dissociation phases are independent of the concentration receptor–ligand complex [41]. Conversely, FTSA measures the manner in which ligands stabilize the tertiary structure of a protein against thermally induced denaturation. This requires micromolar concentrations of protein, which becomes an important factor in determining binding affinities typical of most potential pharmaceutical agents because the concentration of receptor–ligand complex will directly affect the concentration of free ligand [4]. Because the response in this assay is proportional to the concentration of free ligand rather than a saturable effect measured by traditional biochemical assays that measure or infer receptor ligand complex (such as fluorescence polarization and intracellular second messenger assays), it is incorrect to fit these data to a Langmuir isotherm or Hill equations. This is due to the requirements of pseudo-first-order kinetics that govern the Hill equation (i.e., [receptor] ≪ [ligand] so that [receptor–ligand] does not noticeably affect [ligand]) being violated. The Hill equation also requires the response to have an approachable maximum which is in violation of Eq. (5). Despite this, many examples exist in the literature where the use of saturable pseudo-first-order kinetics to analyze FTSA has (incorrectly) been attempted [42,43].

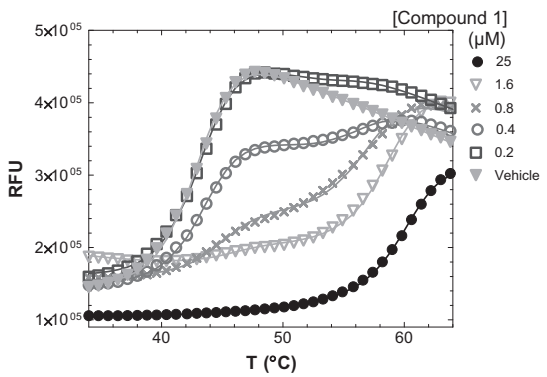

Fig.5. FTSA curves for compound **1**. Measured data are shown as singlicate points representative of three repeats. Measured data are indicated by symbols, with Eq. (3) as a fitted line. The curves were fit according to the biphasic model (Eq. (3)).

To understand the nature by which small molecules may confer an enhanced energy requirement for thermal denaturation and how this energetic requirement is related to compound–protein affinities depends on the value of $\Delta_u H$, the unfolding enthalpy. Ideally this would be measured by DSC [16]; however, in practice it may be estimated from the slope of the unfolding curves in FTSA [4]. This estimation of $\Delta_u H$ has a direct effect on the K_D values ultimately calculated. In this study, the initial estimate for the curves was 100 kJ mol^{-1}; however, this may be retrospectively modified to 60 kJ mol^{-1} to better fit the data. This second value of 60 kJ mol^{-1} also matched much better with data from SPR. Whichever value of $\Delta_u H$ is used, the rank order of the test set of compounds remains unchanged between the two techniques, with the initial estimate of 100 kJ mol^{-1} for $\Delta_u H$ giving K_D values that were within an order of magnitude of those derived by SPR and retaining the ratios of potency between each compound (Fig. 9).

SPR is able to determine, and hence compare, affinities for different set temperatures to derive estimates of thermodynamic parameters via Van't Hoff plots [38]. In addition, estimates of the activation parameters are derived from the association and dissociation constants via Eyring plots [44]. This method of determining ΔH and ΔS has drawbacks in that the actual heat of binding is estimated and not measured. Consequently, at each successive temperature, not only is the interaction between receptor and ligand measured, but also the accompanying interactions involving other components of the system (e.g., water molecules and buffer component metal ions that may also play a role in the interaction) are also measured [45,46]. This leads to discrepancies between

Table 3
Comparison of aggregation properties, affinity, and free energy values obtained using SPR and FTSA methodologies.

Compound number	Purpose	DLS	SPR							FTSA		Literature	
		CAC (M)	K_D (19 °C) (M)	k_a (19 °C) (M^{-1} s^{-1})	k_d (19 °C) (s^{-1})	ΔG_b (kJ mol^{-1})	ΔH_b (kJ mol^{-1})	$T\Delta S_b$ (kJ mol^{-1})	ΔCp (kJ mol^{-1})	K_D (M) 20 °C	ΔG (kJ mol^{-1})	K_D (M)	Method [reference]
1	p38α ligand	7.8e-5 (7.7–7.9e-5)	6.1e-10 (4–8e-10)	8.5e4 (0.6–1e5)	5.2e-5 (5–5.5e-5)	−52	–	–	–	2.53e-10	−53.9 (±1.5)	1e-10	SPR [22]
2	p38α ligand	8.5e-5 (8–9e-5)	5.2e-8 (3–9e-8)	2.2e4 (1–3e-5)	0.001 (0.8–3e-3)	−23	−67 (±3)	−25 (±3)	–	9.67e-8	−39.4 (±0.63)	–	–
3	p38α ligand	–	3.8e-7 (2–7e-7)	2.2e4 (1–3e-5)	0.009 (0.7–1e-2)	−36	−92 (±6)	−55 (±10)	−3 (±2)	1.3e-7	−38.6 (±2.1)	–	–
4	p38α ligand	–	1.1e-6 (0.8–1.5e-6)	2.5e4 (1–3e-5)	0.028 (2–3e-2)	−33	−114 (±6)	−84 (±9)	−4 (±1)	7.93e-7	−34.2 (±0.69)	–	–
5	p38α ligand	–	4.0e-8 (3–5e-8)	6.5e5 (3–8e-5)	0.027 (2–3e-2)	−44	−36 (±2)	8.3 (±4)	–	1.97e-8	−43.2 (±0.69)	3.8e-8	Enzymatic [20]
6	p38α ligand	–	7.8e-8 (0.4–1e-8)	1.7e6 (0.5–3e-5)	0.130 (0.3–2e-1)	−43	−36 (±3)	7.5 (±4)	–	2.47e-8	−42.7 (±0.44)	2.6e-8	ITC [21]
7	p38α ligand	–	5.1e-8 (2–7e-8)	1.3 e6 (1–2e-6)	0.067 (2–9e-2)	−43	−34 (±2)	−9 (±6)	−0.9 (±1)	1.41e-8	−44.1 (±1.49)	4.4e-8	Enzymatic [23]
8	Aggregator	1.6e-5 (1–3e-5)	–	–	–	–	–	–		–	–	–	–
9	Aggregator	2.3e-5 (2–3e-5)	–	–	–	–	–	–		4E-06	–	–	–
10	Chelator	–	–	–	–	–	–	–		–	–	–	–
11	Michael acceptor	–	–	–	–	–	–	–		2E-06	–	–	–
12	Redox cycler	–	–	–	–	–	–	–		–	–	–	–
13	Chelator	–	–	–	–	–	–	–		6E-06	–	–	–

Note. "–" indicates that the compound did not give a reliable result in the assay. The thermodynamic parameters gained from SPR were obtained using Van't Hoff plots. Errors are shown in parentheses; the errors for DLS are the 95% confidence intervals of the fitted data, and the errors for SPR are the confidence intervals taken from three separate measurements. Van't Hoff thermodynamics for SPR is shown as standard errors of the fits, and FTSA errors are the standard errors of the fitted data. Heat capacity was included in the addition of a third parameter and significantly increased the goodness of fit via an *F* test.

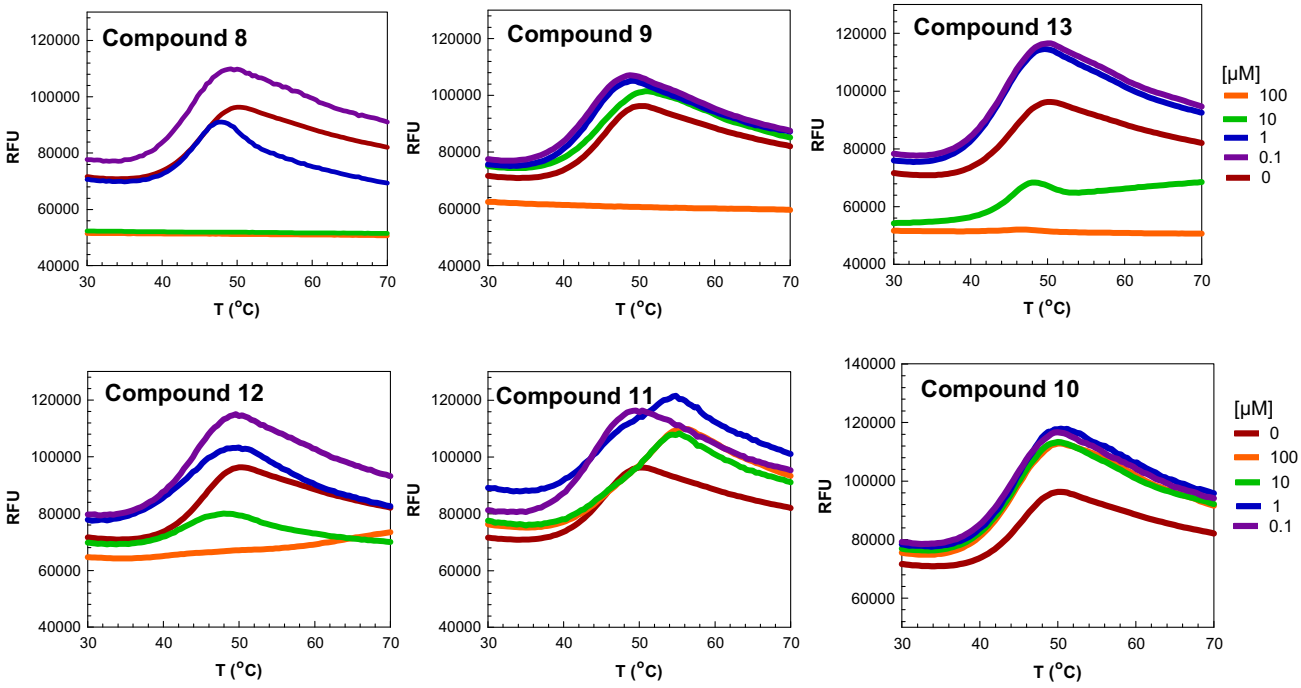

Fig.6. The effects of various PAINs on FTSA assay signal. The panels display fluorescence generated by the SYPRO Orange probe against temperature. All interference compounds cause a decrease in fluorescence without an increase in melting temperature apart from compound **11**, which causes a saturable increase in melting temperature, and compound **10**, which does not affect the protein. Data are singlicate points representative of three repeats.

Van't Hoff-derived thermodynamic parameters and those determined by ITC [45,46], although the parameters obtained for compound **6** match well with those described in Ref. [21]. However, the use of kinetic parameters of binding in Eyring analysis allows for the discrimination of various activation parameters and may allow a better understanding of the events that occur on association and dissociation. For example, unfavorable conformational changes in the small molecules on binding, indicated by unfavorable activation entropy of association [47], or loss and gain of favorable charged interactions, indicated by changes in enthalpic cost of dissociation [48].

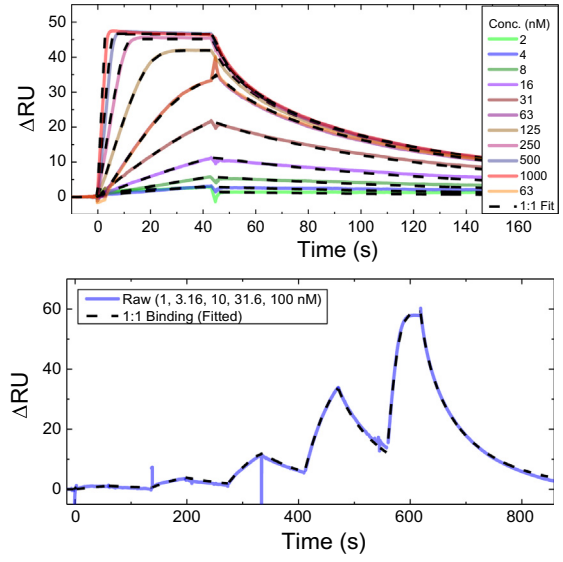

Fig.7. Example data obtained via SPR with multi- and single-cycle kinetics. The top panel shows data for compound **6** run as multi-cycle kinetics with a 1:1 fit shown as black dashed lines. The bottom panel shows single-cycle kinetic data for compound **6**. Data are shown as singlicate points representative of at least two independent runs.

Although ITC remains the gold standard for determining the heat of binding [49], during routine screening of compounds estimates made by techniques such as FTSA and SPR may serve a purpose, much like IC_{50} or EC_{50} values act as an estimate of true K_D values in biochemical screening. FTSA has a much greater throughput with qPCR machines able to generate affinity values at a much reduced protein requirement compared with ITC. Compounds triaged by FTSA may then be prioritized for thermodynamic evaluation by SPR, with the capacity for tens of compounds to be profiled over six temperature points in approximately 24 h using single-cycle kinetics or similar methods (e.g., one step/fast step offered by the SensiQ® Pioneer). This enhanced throughput would allow for logical and predictive testing of compound SAR, such as determining whether increasing the torsional freedom of a small molecule leads to a reduction in entropy [47] and the manner in which various bioisosteres affect the enthalpy of binding [48]. Although the effect of ligand modification on binding thermodynamics might not yet be fully understood as effects such as enthalpy–entropy compensation may occur [50], a medium-throughput technique to generate data across large compound series would be an invaluable tool to help direct medicinal chemistry programs.

As well as discriminating compounds on their ability to bind to proteins, distinguishing small molecules with desirable and undesirable mechanisms is of paramount importance during early-stage drug discovery. Compounds with undesirable mechanisms of inhibition, such as redox cycling [9] (Fig. 3) and promiscuous aggregation [27] (Fig. 2), as well as compounds that interfere with assay technology such as fluorescence quenchers [25], can often be mistaken for potential hit molecules. These molecules have been dubbed as PAINs. To discriminate desirable ligands from PAINs, it is important to understand how they may appear in different

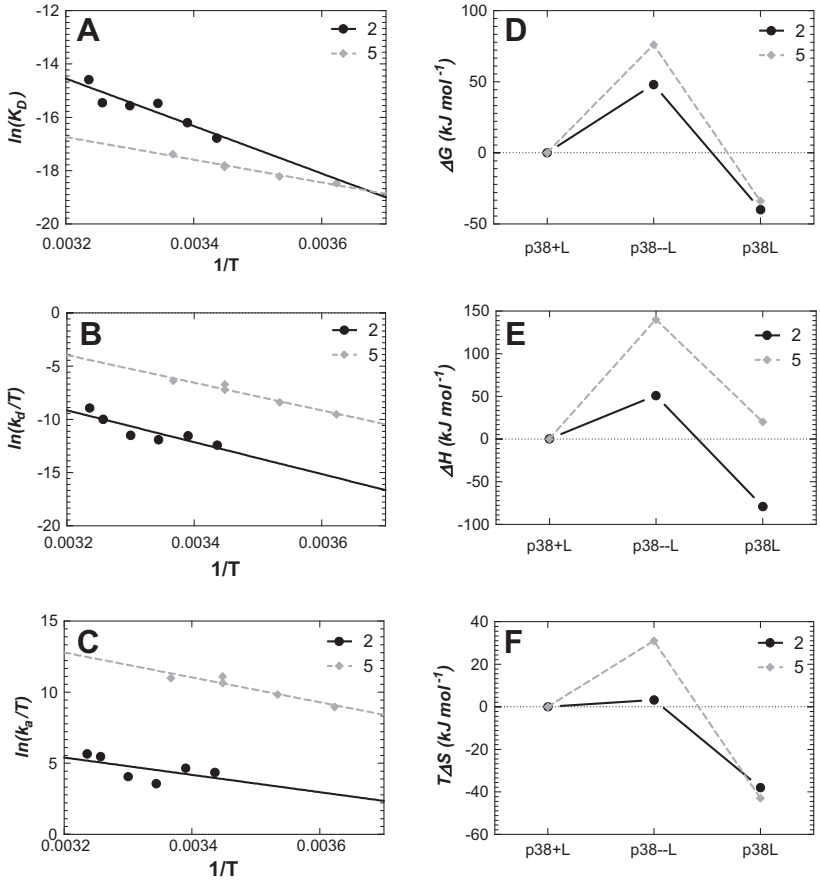

Fig.8. Example thermodynamic data obtained from SPR assays. Panel A shows the Van't Hoff and Eyring plots obtained for compounds **2** and **5**. Panels B and C show Eyring plots for the activation parameters for dissociation and association, respectively. Data shown are the results of a single screen representative of two repeats. Panels D, E, and F show the free energy diagrams obtained from the Eyring analysis of compounds **2** and **5** in terms of the Gibbs free energy change (D), enthalpy change (E), and entropy change (F). In panels D, E, and F, p38+L displays the ground state where the two ligands separate. The difference between p38+L and p38–L is the change on association, and the difference between p38+L and p38L is the change on dissociation; thus the difference between p38–L and p38L is equal to the equilibrium. The data shown are the results of a single screen representative of two repeats.

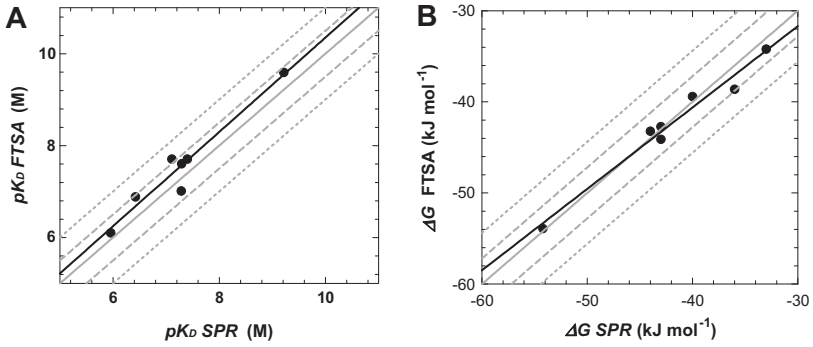

Fig.9. Comparison of affinity and thermodynamic values obtained in SPR and FTSA. In both panels, actual values are indicated by black circles, with the black line representing the general trend. The solid gray line is the line of unity, and the dashed and dotted gray lines represent half an order of magnitude and an order of magnitude deviation from unity in terms of affinity, respectively. Panel A compares affinity values obtained, whereas panel B compares the Gibbs free energy of binding.

technologies. The effect of PAINs in SPR has been described previously in the literature [7], and the results we obtained match well with predictions already made. This is the first time, to our knowledge, that PAINs have been described in FTSA and could serve as a valuable reference for scientists routinely involved in screening via FTSA. DLS is an excellent tool for determining whether compounds aggregate, possibly causing nonspecific inhibition of biological processes. The formation of particles alone is not evidence enough to discard a compound. For example, compounds **1** and **2** both formed particles at the higher concentrations tested (Fig. 2); however, their CAC values were not representative of their measured K_D values, which were more potent by several orders of magnitude, and so it would be incorrect to assume that their binding mechanism was via aggregation. The aggregates seen by DLS for compounds **1** and **2** also had a radius greater than 1000 nm, indicating insolubility rather than aggregation. Compounds **8** and **9** were found to

have CAC values that closely matched their apparent K_D values by FTSA, however, indicating that it was likely aggregation that was responsible for any effects, and so these compounds should be discarded.

In practice, it appears that any compound that lowers the overall fluorescence of FTSA without causing a proportional shift in melting temperature can be discarded because it is likely due to nonspecific mechanisms such as aggregation (compounds **8** and **9**), fluorescence quenching (compound **13**), or fluorophore bleaching (compound **12**) rather than a genuine binding event.

Conclusion

Affinity and thermodynamic values for small molecule ligands to p38α were generated by saturable (SPR) and nonsaturable (FTSA) kinetic methods. Compound values from the two techniques correlated well over four orders of magnitude. Known assay interference compounds were profiled in FTSA, showing responses distinct from true ligands of p38α. The utility of kinetic and thermodynamic information to medicinal chemistry programs was discussed.

References

[1] G. Holdgate, S. Geschwindner, A. Breeze, G. Davies, N. Colclough, D. Temesi, L. Ward, Biophysical methods in drug discovery from small molecule to pharmaceutical, in: M.A. Williams, T. Daviter (Eds.), Protein–Ligand Interactions: Methods and Applications, Methods in Molecular Biology, vol. 1008, Springer, New York, 2013, pp. 327–355.

[2] W. Huber, F. Mueller, Biomolecular interaction analysis in drug discovery using surface plasmon resonance technology, Curr. Pharm. Des. 12 (2006) 3999–4021.

[3] W.H. Ward, G.A. Holdgate, Isothermal titration calorimetry in drug discovery, Prog. Med. Chem. 38 (2001) 309–376.

[4] D. Matulis, J.K. Kranz, F.R. Salemme, M.J. Todd, Thermodynamic stability of carbonic anhydrase: Measurements of binding affinity and stoichiometry using ThermoFluor, Biochemistry 44 (2005) 5258–5266.

[5] S. Perspicace, D. Banner, J. Benz, F. Müller, D. Schlatter, W. Huber, Fragment-based screening using surface plasmon resonance technology, J. Biomol. Screen. 14 (2009) 337–349.

[6] H.L. Silvestre, T.L. Blundell, C. Abell, A. Ciulli, Integrated biophysical approach to fragment screening and validation for fragment-based lead discovery, Proc. Natl. Acad. Sci. U.S.A. 110 (2013) 12984–12989.

[7] A.M. Giannetti, B.D. Koch, M.F. Browner, Surface plasmon resonance based assay for the detection and characterization of promiscuous inhibitors, J. Med. Chem. 51 (2008) 574–580.

[8] M.F. Sassano, A.K. Doak, B.L. Roth, B.K. Shoichet, Colloidal aggregation causes inhibition of G protein-coupled receptors, J. Med. Chem. 56 (2013) 2406–2414.

[9] L.A. Lor, J. Schneck, D.E. McNulty, E. Diaz, M. Brandt, S.H. Thrall, B. Schwartz, A simple assay for detection of small-molecule redox activity, J. Biomol. Screen. 12 (2007) 881–890.

[10] R.A. Copeland, D.L. Pompliano, T.D. Meek, Drug–target residence time and its implications for lead optimization, Nat. Rev. Drug Discov. 5 (2006) 730–739.

[11] Y. Kawasaki, E. Freire, Finding a better path to drug selectivity, Drug Discov. Today 16 (2011) 985–990.

[12] J.E. Ladbury, G. Klebe, E. Freire, Adding calorimetric data to decision making in lead discovery: a hot tip, Nat. Rev. Drug Discov. 9 (2010) 23–27.

[13] A.D. Scott, C. Phillips, A. Alex, M. Flocco, A. Bent, A. Randall, R. O'Brien, L. Damian, L.H. Jones, Thermodynamic optimisation in drug discovery: a case study using carbonic anhydrase inhibitors, ChemMedChem 4 (2009) 1985–1989.

[14] M.R. Duff Jr., J. Grubbs, E.E. Howell, Isothermal titration calorimetry for measuring macromolecule–ligand affinity, J. Vis. Exp 55 (2011).

[15] K. Park, J.M. Lee, Y. Jung, T. Habtemariam, A.W. Salah, C.D. Fermin, M. Kim, Combination of cysteine- and oligomerization domain-mediated protein immobilization on a surface plasmon resonance (SPR) gold chip surface, Analyst 136 (2011) 2506–2511.

[16] J.F. Brandts, L.N. Lin, Study of strong to ultratight protein interactions using differential scanning calorimetry, Biochemistry 29 (1990) 6927–6940.

[17] A. Zubrienė, J. Matulienė, L. Baranauskienė, J. Jachno, J. Torresan, V. Michailovienė, P. Cimmperman, D. Matulis, Measurement of nanomolar dissociation constants by titration calorimetry and thermal shift assay: Radicicol binding to Hsp90 and ethoxzolamide binding to CAII, Int. J. Mol. Sci. 10 (2009) 2662–2680.

[18] P. Cimmperman, L. Baranauskienė, S. Jachimoviciūte, J. Jachno, J. Torresan, V. Michailovienė, J. Matulienė, J. Sereikaite, V. Bumelis, D. Matulis, A quantitative model of thermal stabilization and destabilization of proteins by ligands, Biophys J. 95 (2008) 3222–3231.

[19] F.H. Niesen, H. Berglund, M. Vedadi, The use of differential scanning fluorimetry to detect ligand interactions that promote protein stability, Nat. Protoc. 2 (2007) 2212–2221.

[20] S.P. Davies, H. Reddy, M. Caivano, P. Cohen, Specificity and mechanism of action of some commonly used protein kinase inhibitors, Biochem. J. 351 (2000) 95–105.

[21] G.F. De Nicola, E.D. Martin, A. Chaikuad, R. Bassi, J. Clark, L. Martino, S. Verma, P. Sicard, R. Tata, R.A. Atkinson, S. Knapp, M.R. Conte, M.S. Marber, Mechanism and consequence of the autoactivation of p38α mitogen-activated protein kinase promoted by TAB1, Nat. Struct. Mol. Biol. 20 (2013) 1182–1190.

[22] J. Regan, C.A. Pargellis, P.F. Cirillo, T. Gilmore, E.R. Hickey, G.W. Peet, A. Proto, A. Swinamer, N. Moss, The kinetics of binding to p38MAP kinase by analogues of BIRB 796, Bioorg. Med. Chem. Lett. 13 (2003) 3101–3104.

[23] D.C. Underwood, R.R. Osborn, C.J. Kotzer, J.L. Adams, J.C. Lee, E.F. Webb, D.C. Carpenter, S. Bochnowicz, H.C. Thomas, D.W. Hay, D.E. Griswold, SB 239063, a potent p38 MAP kinase inhibitor, reduces inflammatory cytokine production, airways eosinophil infiltration, and persistence, J. Pharmacol. Exp. Ther. 293 (2000) 281–288.

[24] J. Seidler, S.L. McGovern, T.N. Doman, B.K. Shoichet, Identification and prediction of promiscuous aggregating inhibitors among known drugs, J. Med. Chem. 46 (2003) 4477–4486.

[25] K.L. Vedvik, H.C. Eliason, R.L. Hoffman, J.R. Gibson, K.R. Kupcho, R.L. Somberg, K.W. Vogel, Overcoming compound interference in fluorescence polarization-based kinase assays using far-red tracers, Assay Drug Dev. Technol. 2 (2004) 193–203.

[26] N. Thorne, D.S. Auld, J. Inglese, Apparent activity in high-throughput screening: origins of compound-dependent assay interference, Curr. Opin. Chem. Biol. 14 (2010) 315–324.

[27] K.E.D. Coan, D.A. Maltby, A.L. Burlingame, B.K. Shoichet, Promiscuous aggregate-based inhibitors promote enzyme unfolding, J. Med. Chem. 52 (2009) 2067–2075.

[28] D. Matulis, C. Wu, T. Van Pham, C. Guy, R. Lovrien, Protection of enzymes by aromatic sulfonates from inactivation by acid and elevated temperatures, J. Mol. Catal. B 7 (1999) 21–36.

[29] R.S. Ferreira, C. Bryant, K.K.H. Ang, J.H. McKerrow, B.K. Shoichet, A.R. Renslo, Divergent modes of enzyme inhibition in a homologous structure–activity series, J. Med. Chem. 52 (2009) 5005–5008.

[30] F. Guillen, A.T. Martínez, M.J. Martínez, C.S. Evans, Quinone redox cycling in the ligninolytic fungus *Pleurotus eryngii* leading to extracellular production of superoxide anion radical, Arch. Biochem. Biophys. 339 (1997) 190–199.

[31] H.B. Kramer, B. Nicholson, B.M. Kessler, M. Altun, Detection of ubiquitin–proteasome enzymatic activities in cells: application of activity-based probes to inhibitor development, Biochim. Biophys. Acta 2012 (1823) 2029–2037.

[32] M.J. Miller, Syntheses and therapeutic potential of hydroxamic acid based siderophores and analogs, Chem. Rev. 89 (1989) 1563–1579.

[33] M. Kaszuba, D. McKnight, M.T. Connah, F.K. McNeil-Watson, U. Nobbmann, Measuring sub nanometre sizes using dynamic light scattering, J. Nanopart. Res. 10 (2008) 823–829.

[34] D. Hammaker, G.S. Firestein, "Go upstream, young man": lessons learned from the p38 saga, Ann. Rheum. Dis. 69 (Suppl. 1) (2010) i77–i82.

[35] S. Kumar, J. Boehm, J.C. Lee, P38 MAP kinases: key signalling molecules as therapeutic targets for inflammatory diseases, Nat. Rev. Drug Discov. 2 (2003) 717–726.

[36] J.D. Ashwell, The many paths to p38 mitogen-activated protein kinase activation in the immune system, Nat. Rev. Immunol. 6 (2006) 532–540.

[37] R.Y. Liu, C. Fan, G. Liu, N.E. Olashaw, K.S. Zuckerman, Activation of p38 mitogen-activated protein kinase is required for tumor necrosis factor-α-supported proliferation of leukemia and lymphoma cell lines, J. Biol. Chem. 275 (2000) 21086–21093.

[38] D. Casper, M. Bukhtiyarova, E.B. Springman, A Biacore biosensor method for detailed kinetic binding analysis of small molecule inhibitors of p38α mitogen-activated protein kinase, Anal. Biochem. 325 (2004) 126–136.

[39] J. Regan, Structure–activity relationships of the p38α MAP kinase inhibitor 1-(5-*tert*-butyl-2-*p*-tolyl-2H-pyrazol-3-yl)-3-[4-(2-morpholin-4-yl-ethoxy)naphthalen-1-yl]urea (BIRB 796), J. Med. Chem. 46 (2003) 4676–4686.

[40] R.R. Kroe, Thermal denaturation: a method to rank slow binding, high-affinity p38α MAP kinase inhibitors, J. Med. Chem. 46 (2003) 4669–4675.

[41] D.J. O'Shannessy, D.J. Winzor, Interpretation of deviations from pseudo-first-order kinetic behavior in the characterization of ligand binding by biosensor technology, Anal. Biochem. 236 (1996) 275–283.

[42] M. Vivoli, H.R. Novak, J.A. Littlechild, N.J. Harmer, Determination of protein–ligand interactions using differential scanning fluorimetry, J. Vis. Exp 91 (2014). 10.3791/51809 e51809.

[43] N. Boucher, K.M. Noll, Ligands of thermophilic ABC transporters encoded in a newly sequenced genomic region of *Thermotoga maritima* MSB8 screened by differential scanning fluorimetry, Appl. Environ. Microbiol. 77 (2011) 6395–6399.

[44] Y.S. Day, C.L. Baird, R.L. Rich, D.G. Myszka, Direct comparison of binding equilibrium, thermodynamic, and rate constants determined by surface- and solution-based biophysical methods, Protein Sci. 11 (2002) 1017–1025.

[45] G. Zeder-Lutz, E. Zuber, J. Witz, M.H. Van Regenmortel, Thermodynamic analysis of antigen–antibody binding using biosensor measurements at different temperatures, Anal. Biochem. 246 (1997) 123–132.

[46] H. Roos, R. Karlsson, H. Nilshans, A. Persson, Thermodynamic analysis of protein interactions with biosensor technology, J. Mol. Recognit. 11 (1998) 204–210.

[47] C.-E.A. Chang, W. Chen, M.K. Gilson, Ligand configurational entropy and protein binding, Proc. Natl. Acad. Sci. U.S.A. 104 (2007) 1534–1539.
[48] C. Bissantz, B. Kuhn, M. Stahl, A medicinal chemist's guide to molecular interactions, J. Med. Chem. 53 (2010) 5061–5084.
[49] A. Zubrienė, E. Kazlauskas, L. Baranauskiene, V. Petrauskas, D. Matulis, Isothermal calorimetry and thermal shift assay in drug design, Eur. Pharm. Rev. 16 (2011) 56–59.
[50] A. Cornish-Bowden, Enthalpy–entropy compensation: a phantom phenomenon, J. Biosci. 27 (2002) 121–126.